Appendix

The spatial density distribution of molecules at various time delays after their desorption can be calculated from their initial speed and angular distributions. Let $\rho(r,\Omega_r)$ be the density at a distance r and direction Ω, then

$$\rho(r,\Omega_r)r^2\,dr\,d\Omega_r = R(r)\,I(\Omega_r)r^2\,dr\,d\Omega_r$$

represents the number in a unit solid angle $d\Omega_r$ at Ω_r and between r and $r + dr$. For the case of a pulsed point source on a surface, the density of desorbing molecules is associated with the desorption speed distribution $N(v)$, angular distribution $I(\Omega_v)$, and delay time t_d. Since $r = vt_d$, and $\Omega_r = \Omega_v = \Omega$, we have

$$R(r)\,I(\Omega_r)r^2\,dr\,d\Omega_r = N(v)\,I(\Omega_v)v^2\,dv\,d\Omega_v$$
$$= N(r/t_d)I(\Omega)r^2\,dr\,d\Omega/t_d^3 \quad (11)$$

Thus, the number of molecules in any region above the surface is obtained by integrating $R(r)\,I(\Omega)$ over that region. The normalized angular distribution can be described as

$$I(\Omega) = (n + 1)/2\pi\cos^n\theta \quad (12)$$

If the normalized speed distribution is assumed to be Maxwell-Boltzmann, then

$$N(v)v^2\,dv = N_{MB}(v)\,dv$$
$$= 4\pi(m/2\pi kT)^{3/2}v^2\exp(-mv^2/2kT)\,dv \quad (13)$$

Thus, the fraction of the total number of desorbed molecules within some region above the surface at a time t_d is

$$F = \int_r\int_\Omega R(r)\,I(\Omega)r^2\,dr\,d\Omega$$
$$= \int_r\int_\theta\int_\phi \frac{2(n+1)(m/2\pi kT)^{3/2}}{t_d^3}\times$$
$$\exp(-mr^2/2kTt_d^2)\cos^n\theta r^2\,dr\sin\theta\,d\theta\,d\phi \quad (14)$$

Figure 9 illustrates the regions in which the molecular density has been calculated. Under our experimental conditions the flight time of ions to the detector is approximately 18 μs, and the diameter of the detector face is 18 mm. Therefore, molecules having a perpendicular velocity component larger than 500 m/s are not detected. This implies that at a delay time of 70 ns following the desorption pulse molecules that have traveled further than 35 μm in a direction perpendicular to the ion flight tube axis will not be detected. This implies that for a 70-ns delay the effective ionization regions are cylindrical disks with radii of 35 μm. (For a longer delay the radii are correspondingly larger.) Calculations are performed for disks of 1-μm thickness. For the numerical integration, each disk was divided into 900 rings in which the numbers of molecules at different speeds are calculated and summed up. The calculated number of desorbed molecules in 35-μm-diameter cylindrical disks at various distances from the surface is displayed in Figure 3 for three different temperatures and three different angular distributions.

C-C and C-H Bond Splits of Laser-Excited Aromatic Molecules. 1. Specific and Thermally Averaged Rate Constants

U. Brand, H. Hippler, L. Lindemann, and J. Troe*

Institut für Physikalische Chemie der Universität Göttingen, Tammannstrasse 6, D-3400 Göttingen, West Germany *(Received: August 17, 1989; In Final Form: February 14, 1990)*

Toluene, *m*-, *o*-, and *p*-xylene, mesitylene, ethyl-, isopropyl-, and *tert*-butylbenzene were irradiated by nanosecond laser flashes at 193 nm. After fast internal conversion to the electronic ground state, the molecules dissociate by C-C or C-H bond splits. The products of the fragmentation were identified by comparison with the UV spectra of products from the photolysis of the corresponding α-bromoalkylbenzenes. Toluene, the xylenes, and mesitylene predominantly dissociate by C-H bond split in the methyl groups, the α-methyl-substituted toluenes dissociate by C-C bond split into methyl + substituted benzyl radicals. Specific rate constants $k(E,J)$ for the dissociations were determined in low-pressure experiments with an extrapolation to zero pressure. Statistical adiabatic channel (SACM) calculations of $k(E,J)$ are fitted to the experiments and used to calculate the corresponding high-pressure rate constants for thermal dissociation and recombination.

1. Introduction

The study of the pyrolysis of aromatic molecules under combustion conditions has presented a number of experimental problems which are difficult to overcome: (i) the primary reaction can be governed by a competition of C-H and C-C bond splits; (ii) secondary reactions can lead to complicated mechanisms; (iii) the falloff curves of the unimolecular bond fission are so broad that extrapolations to the limiting low- and high-pressure rate constants are difficult to perform (see refs 1-3 and work cited therein). Laser excitation experiments offer an elegant way out of this dilemma. The photophysics of aromatic molecules, under irradiation at suitable wavelengths in the UV region, is governed by sufficiently fast internal conversions from excited electronic states to the ground state. In this way energy-selected molecules can be prepared whose vibrational excitation is of the same order as in high-temperature thermal excitation situations. By working with isolated molecules one can directly identify the primary dissociation products; branching ratios and specific dissociation rate constants are measured. The isolated molecule data then can be converted to thermal reaction data by using modern unimolecular rate theory. An example of this procedure has been given in ref 2 for the dissociation of toluene. The present work extends this approach to other alkyl-substituted benzenes such as those frequently encountered in today's fuels. It also discusses in more detail the theoretical connections between specific rate constants from laser excitation experiments and thermally averaged rate constants under pyrolysis conditions.

The first direct study of a simple bond fission after laser excitation was reported in ref 4 where vibrationally highly excited toluene ($E \approx 623$ kJ mol^{-1} ≅ 52080 cm^{-1}) in the electronic ground

(1) Müller-Markgraf, W. Troe, J. *J. Phys. Chem.* **1988**, *92*, 4899.
(2) Brouwer, L. D.; Müller-Markgraf, W.; Troe, J. *J. Phys. Chem.* **1988**, *92*, 4905.
(3) Müller-Markgraf, W.; Troe, J. *J. Phys. Chem.* **1988**, *92*, 4914.
(4) Hippler, H.; Schubert, V.; Troe, J.; Wendelken, H. J. *Chem. Phys. Lett.* **1981**, *84*, 253.

0022-3654/90/2094-6305$02.50/0

state was produced by electronic excitation of the isomer cycloheptatriene at 248 nm followed by fast internal conversion and unimolecular isomerization. Under the chosen conditions a specific rate constant of about 3×10^6 s^{-1} (uncertainty of a factor of 2) was measured by monitoring the overlapping UV absorption continua of hot toluene and hot fragment radicals. Accidentally, electronic excitation of toluene at 193 nm with subsequent internal conversion produces vibrationally highly excited toluene of practically the same internal energy as the excitation of cycloheptatriene at 248 nm. The measurement of a rate coefficient of 2.4×10^6 s^{-1} for benzyl formation,[5] therefore, confirms a mechanism involving the electronic ground state in both cases. The rate coefficients for hydrogen atom formation[6] from cycloheptatriene excitation at 248 nm (2.6×10^6 s^{-1}) or toluene excitation at 193 nm (3×10^6 s^{-1}) agree with these data such that an internally consistent picture arises.

The first direct detection of competing C–C and C–H bond splits in toluene dissociation was achieved in molecular beams where C–H bond split was identified to be the major channel.[7] The properties of this branching are of interest in relation to statistical unimolecular rate theory. In addition, there is practical relevance of this problem since different reaction products may influence the secondary mechansim in different ways. For this reason, we have undertaken a careful investigation of the branching ratios for C–H and C–C bond splits in the present work, as well as in part 2 of this series.[8] The branching ratios depend on the energy E and the angular momentum J. As a consequence, the thermal reaction will be characterized by temperature (and pressure)-dependent branching ratios.[9] This behavior will be discussed for the present system in part 2.[8]

Larger alkyl-substituted benzenes have been studied in less detail. There are similar uncertainties as for toluene with the thermal pyrolysis rates and the identification of the primary dissociation fragments and their detailed branching ratios. Laser excitation experiments again provide more conclusive answers. Rates of benzyl formation after excitation at 193 nm of ethylbenzene (2×10^7 s^{-1}), propylbenzene (6.6×10^6 s^{-1}), and butylbenzene (2.2×10^6 s^{-1}) were reported in ref 5. Further studies with partially deuterated toluenes, ethylbenzenes and butylbenzenes in ref 10 continued this work, slightly modified the rates (2.6×10^7 s^{-1} for ethylbenzene and 1.6×10^6 s^{-1} for butylbenzene), and confirmed the statistical character of the dissociation process. Since benzyl spectra were observed, predominantly C–C bond split was assumed for ethyl-, propyl-, and butylbenzene dissociation. After excitation of *p*-xylene at 193 nm, the rate constant for H atom formation was reported in ref 6, suggesting predominant C–H bond split in this case such as also observed for the other xylenes and mesitylene.[11] The experiments from ref 11 indicated about 1 order of magnitude decrease of the rate constant per added methyl group in the series methyl-, dimethyl-, and trimethylbenzene. This result is similar to our earlier observations for isomerization of alkyl-substituted cycloheptatrienes; see ref 12. The present article, extending earlier work from refs 13 and 14, describes measurements for a series of C–H and C–C bond splits in more detail, comparing the measured specific rate constants with statistical adiabatic channel calculations (SACM in the version of ref 15). Earlier simple RRKM calculations in other studies neglected the J-dependence of $k(E,J)$ and, therefore, are not suitable for a conversion into high-temperature pyrolysis constants. The present SACM treatment allows for a realistic analysis of the possibilities and limitations of the conversion between laser excitation and thermal rate data.

The present work also systematically analyzes the spectra of the major dissociation products by comparison with radical spectra from the corresponding radical bromide photolysis. The conclusions from the kinetic studies on the dominant dissociation pathway are supported in this way. The quantitative determination of the product yield from the minor pathways by a multiphoton ionization technique is given in part 2[8] together with a SACM representation of the energy-specific and thermally averaged branching ratios.

Part 3[16] of this series applies our recent UV multiphoton excitation technique[17] to the toluene system. Laser intensity and pressure dependences of the product yields are interpreted in terms of the previous results on excited-state absorption cross sections,[18] collisional energy transfer,[19] and specific rate constants from the present work. In this way it extends the most recent UV multiphoton excitation study with toluene from ref 20. Competing C–H and C–C bond splits may become particularly important in multiphoton excitation experiments when large energies are involved. Therefore, multiphoton excitation studies provide a most useful extension of the dissociation experiments such as discussed in part 3.[16]

2. Experimental Technique

In the present work alkylbenzenes were irradiated with 15-ns pulses from an ArF excimer laser at 193 nm (Lambda Physik EMG 102, pulse energies of 40–50 mJ). After the laser pulse, absorption–time profiles of the excited molecules and the reaction products were recorded over the spectral range 220–320 nm. The light source for the absorption measurement was a Xe–Hg high-pressure arc lamp (Hanovia 910-C-1, 150 W) whose intensity was increased by a factor of 500 for a period of 100 μs by using a suitable lamp pulser. The laser excitation and lamp analysis light beams were transmitted coaxially through a reaction cell of 50 cm length and 2.5 cm inner diameter. The analysis light was dispersed behind the cell in a quartz prism double monochromator (Zeiss MM3) and recorded with a photomultiplier (RCA 1P28A) and a transient digitizer (Tektronix TD7912). Averaging of large numbers of experiments was possible in this way. In each case, the intensity profile of the analysis light pulses before entering the cell was also recorded. Laser pulse energies were measured as well by using a pyroelectrical detector (GenTec ED200). The recorded data were all handled in a PDP 11/34 computer. The optical arrangement was carefully optimized to reduce stray light from the laser as much as possible. Further details of our setup have been described in earlier reports such as refs 12, 18, and 19.

The substances investigated were supplied from Fluka (toluene) or Aldrich (all other compounds). They were of better than 99% purity (better than 97% for the bromides). The substances were carefully distilled, degassed, and introduced as a slow flow through the reaction cell. The analysis light usually was blocked from the cell by an electrical shutter. Its opening triggered the lamp pulser; after the plateau of the analysis light was reached, the excitation laser was fired. Finally, the electrical shutter was closed again

(5) Ikeda, N.; Nakashima, N.; Yoshihara, K. *J. Chem. Phys.* **1985**, *82*, 5285.
(6) Tsukiyama, K.; Bersohn, R. *J. Chem. Phys.* **1987**, *86*, 745.
(7) Krajnovich, D. J.; Buss, R. J.; Lee, Y. T. Presented at the XV International Conference on Photochemistry, Stanford, CA, 1982. Krajnovich, D. J. Ph.D. Thesis, University of California, Berkeley, 1983. Brudzynski, R. J.; Felder, P.; Buss, R. J.; Lee, Y. T. Presented at the International Conference on Radiationless Transitions, Newport Beach, CA, 1984. Brudzynski, R. J. Ph.D. Thesis, University of California, Berkeley, 1987.
(8) Luther, K.; Troe, J.; Weitzel, K. M. *J. Phys. Chem.*, in this issue (part 2).
(9) Just, Th.; Troe, J. *J. Phys. Chem.* **1980**, *84*, 3068.
(10) Kajii, Y.; Obi, K.; Tanaka, I.; Ikeda, N.; Nakashima, N.; Yoshihara, K. *J. Chem. Phys.* **1987**, *86*, 6115.
(11) Bersohn, R. Private communication, December 1987.
(12) Hippler, H.; Luther, K.; Troe, J.; Wendelken, H. J. *Chem. Phys.* **1983**, *78*, 239.
(13) Brand, U. Diplomarbeit, Göttingen, 1986. Lindemann, L. Dissertation, Göttingen, 1987.
(14) Hippler, H.; Lindemann, L.; Troe, J. *Ber. Bunsen-Ges. Phys. Chem.* **1988**, *92*, 440.
(15) Troe, J. *J. Chem. Phys.* **1983**, *79*, 6017.
(16) Hippler, H.; Riehn, C.; Troe, J.; Weitzel, K.-M. *J. Phys. Chem.*, in this issue (part 3).
(17) Damm, M.; Hippler, H.; Troe, J. *J. Chem. Phys.* **1988**, *88*, 3564.
(18) Hippler, H.; Troe, J.; Wendelken, H. J. *J. Chem. Phys.* **1983**, *78*, 5351.
(19) Hippler, H.; Troe, J.; Wendelken, H. J. *J. Chem. Phys.* **1983**, *78*, 6709, 6718.
(20) Nakashima, N.; Ikeda, N.; Yoshihara, K. *J. Phys. Chem.* **1988**, *92*, 4389.

until a new experiment was started and recorded.

3. Experimental Observations and Their Evaluation

In our experiments the reacting molecules were studied under varying pressures, either undiluted or in the presence of an excess of N_2. After laser excitation at 193 nm, absorption–time profiles were recorded for a large number of wavelengths (about every 5 nm in the range 220–320 nm). The absorption–time profiles showed a number of general features such as those described in the following.

(i) At sufficiently low pressures of the reacting molecules, often there was an absorption step during the laser pulse which, on a much slower time scale, was followed by an exponential approach to a steady final absorption level. The initial absorption step is due to population of absorbing vibrationally excited parent molecules generated by the laser beam. Hot UV absorption continua of the parent molecules corresponding to these absorption steps have been studied before such as described, e.g., in ref 18. The absorptions of the highly vibrationally excited parent molecules during their dissociation decrease exponentially with time and are replaced by hot UV absorption of the dissociation products which grow corresponding to the same rate law. The resulting superimposed absorption signals could all be represented by first-order rate laws with apparent first-order rate coefficients $k_{eff}(P)$. These depend on the pressure P such that an extrapolation toward zero pressure always had to be performed. Likewise, the final absorption levels, which correspond to the quantum yield $\phi(P)$ of the dissociation process, depend on the pressure. The pressure dependences of $k_{eff}(P)$ and $\phi(P)$ are governed by the competition between unimolecular dissociation and collisional deactivation such as discussed in ref 21 and, therefore, are linked. Under the conditions where linear Stern–Volmer plots are approached, a representation of the absorption signals $S(t)$ after the initial absorption step following

$$S(t) \approx S(t=\infty) + [S(t=0) - S(t=\infty)] \exp(-k_{eff}(P)t) \quad (1)$$

with

$$k_{eff}(P) \approx k(E_{ac}) + \gamma_c Z_{LJ} P \quad (2)$$

appears appropriate.[21] Here $S(t)$ denotes the difference between the transmitted light intensity after the laser pulse at the time t and before the pulse (small signals were always obtained). Likewise, the final absorption levels

$$S(t=\infty,P) \propto P\phi(P) \quad (3)$$

in the limit $P \rightarrow 0$ can be represented with a quantum yield

$$\phi(P)/\phi(P\rightarrow 0) \approx k(E_{ac})/\{k(E_{ac}) + \gamma_c Z_{LJ} P\} \quad (4)$$

In these equations $k(E_{ac})$ is the specific rate constant of the unimolecular reaction at the initial excitation energy E_{ac}, Z_{LJ} is the Lennard-Jones collision frequency, P is the pressure of the parent molecule, and γ_c is a "collision efficiency" depending on E_{ac} such as discussed in ref 21. In the presence of inert bath gases, their contribution has to be added to the pressure dependent terms in eqs 2 and 4. It should be emphasized that $\phi(P\rightarrow 0)$ is not yet specified in eqs 3 and 4.

(ii) The final absorption levels and their wavelength dependence, in the limit $P\rightarrow 0$, can serve for an identification of the dissociation fragments and their yields. The identification is done by comparison of the spectra with those of the fragments from the photolysis of the corresponding bromides, e.g., benzyl bromide in the dissociation of ethylbenzene to benzyl + CH_3. In practice, only the dominant dissociation fragments could be identified in this way. A determination of the absolute yield of the dominant dissociation fragment requires the knowledge of the fragment absorption coefficient ϵ under the conditions of the dissociation experiment. The relevant halide molecules, by analogy to the alkylbenzenes, are known to photodissociate, forming vibrationally excited products[22,23] such that excited-dependent hot UV absorptions of the dissociation products arise as well. Therefore, a determination of the absolute yields of the dominant fragments from alkylbenzene dissociations can only be achieved to the extent that the hot radical absorption coefficients can be calibrated from the bromide photolysis experiments. A measurement of the yields of the minor photolysis channels, such as done in part 2,[8] leads to a more precise determination of the yields of the major channels. Nevertheless, the present yield measurements at least are semiquantitative and allow for a clear identification of the major dissociation pathway. This observation then can be compared with conclusions drawn on the basis of the absolute values of $k(E_{ac})$.

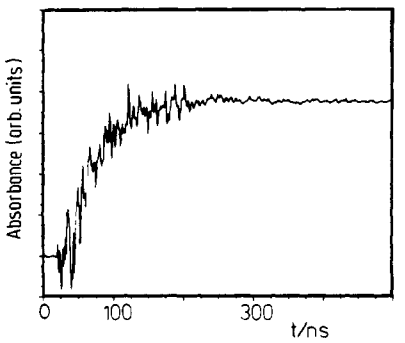

Figure 1. Absorption–time profile of benzyl formation during the dissociation of ethylbenzene (ethylbenzene pressure = 110 mTorr; photolysis wavelength = 193.3 nm; observation wavelength = 266 nm).

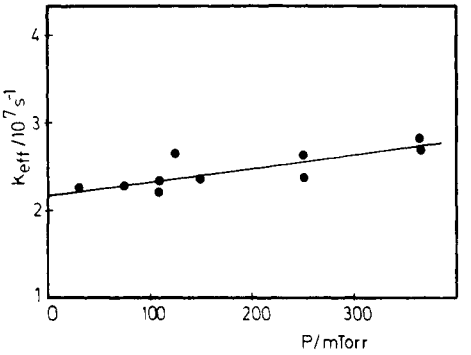

Figure 2. First-order rate coefficient k_{eff} of benzyl formation in the dissociation of ethylbenzene (P = ethylbenzene pressure; photolysis wavelength = 193.3 nm).

(iii) With increasing pressure one observes a change in the absorption–time profiles: the absorption levels reached by the dissociation do not stay constant but show a further change toward lower or higher final values. This effect is produced by collisional deactivation of the hot photolysis fragments as well as those hot parent molecules for which reaction was quenched by collisions. Since this "cooling of the spectrum" generally requires many more collisions than the quenching of the photolysis, absorption changes due to the reaction and due to the cooling of the spectrum can well be separated. A quantitative analysis of this phenomenon was given before in ref 12. With sufficiently fast primary dissociation, relatively high pressures of added N_2 cool the radical spectra so fast that the room temperature spectra can also be analyzed without quenching of the primary photolysis or interference from secondary reactions such as recombination.

Examples of the recorded absorption–time profiles for various pressures and wavelengths will be shown below together with the description of individual reaction systems.

4. Experimental Results

4.1. Ethylbenzene. Figure 1 shows a typical absorption–time profile recorded at the wavelength 266 nm after the 193.3-nm excitation of 110 mTorr of ethylbenzene. In this case there is practically no initial absorption step, i.e., $S(t=0) = 0$. The figure shows the result of an averaging of 200 runs. The "noise" of the

(21) Troe, J. *J. Phys. Chem.* **1983**, *87*, 1800.
(22) Ichimura, T. *J. Chem. Soc., Faraday Trans. 2* **1986**, *82*, 2153.
(23) Freedman, A.; Yang, S. C.; Kawasaki, M.; Bersohn, R. J. *J. Chem. Phys.* **1980**, *72*, 1028.

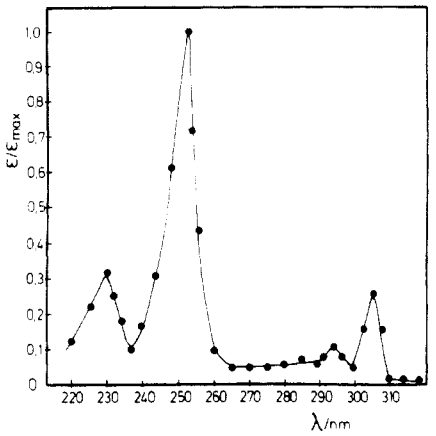

Figure 3. Spectrum of benzyl radicals from ethylbenzene photolysis (recorded after 10 μs with "cooling" by 7 Torr of N_2).

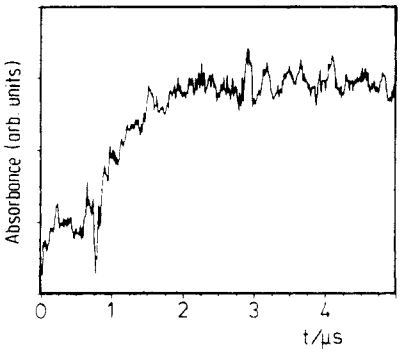

Figure 4. Absorption–time profile of benzyl formation during the dissociation of toluene (toluene pressure = 18 mTorr; photolysis at 193.3 nm; observation at 266 nm).

first part of the signal is due to some electrical pick up from the laser discharge. The signal follows the rate law of eq 1. Figure 2 shows the weak but nevertheless detectable pressure dependence of $k_{eff}(P)$. Extrapolation to zero pressure gives $k(E_{ac}) = (2.3 \pm 0.2) \times 10^7$ s^{-1} where $E_{ac} = 52960$ cm^{-1} corresponds to the photon energy plus the initial average thermal energy at room temperature (1230 cm^{-1}).

Because of the high rate of ethylbenzene dissociation, "cooling" of the fragment spectrum responsible for the signal in Figure 1 could be investigated by adding N_2. With 7 Torr of N_2 the cooling of the spectrum was complete within about 10 μs. Figure 3 shows the resulting spectrum. It coincides in all details with the spectrum of the benzyl radical produced[24] by benzyl chloride photolysis and cooling of the spectrum in the presence of 800 Torr of N_2. The yield of the benzyl radicals from ethylbenzene dissociation can be estimated quantitatively on the basis of the ethylbenzene absorption coefficient $\epsilon = 5000$ L mol^{-1} cm^{-1} at the laser wavelength 193.3 nm (measured in this work with a Cary 17D spectrometer), the measured incident laser energy, the room temperature benzyl absorption coefficient[24] $\epsilon = 25000$ L mol^{-1} cm^{-1} at the absorption maximum at 253 nm, and the reduction of the ethylbenzene dissociation yield to $\phi(P)/\phi(P=0) = 0.8$ by a nitrogen pressure of 7 Torr (estimated on the basis of energy-transfer data for nitrogen and toluene from ref 19). In this way one obtains a primary benzyl yield from ethylbenzene dissociation of more than 0.75 clearly identifying the C–C bond split to benzyl as the dominant dissociation pathway. The shape of the benzyl spectrum strongly depends on the vibrational excitation of the radical. Therefore, quite different absorption–time profiles are recorded at different wavelengths during the cooling of the spectrum.

4.2. Toluene. After excitation at 193.3 nm, toluene dissociates on a much slower time scale than ethylbenzene. Figures 4 and 5 show two typical signals recorded at 266 nm with initial toluene

(24) Ikeda, N.; Nakashima, N.; Yoshihara, K. *J. Phys. Chem.* **1984**, *88*, 5803.

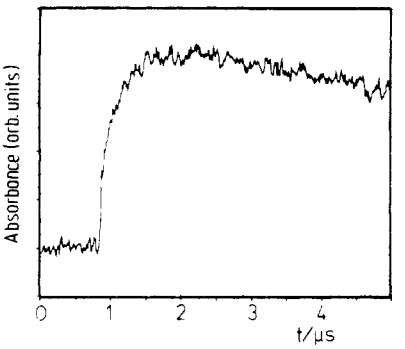

Figure 5. As Figure 4, toluene pressure = 120 mTorr.

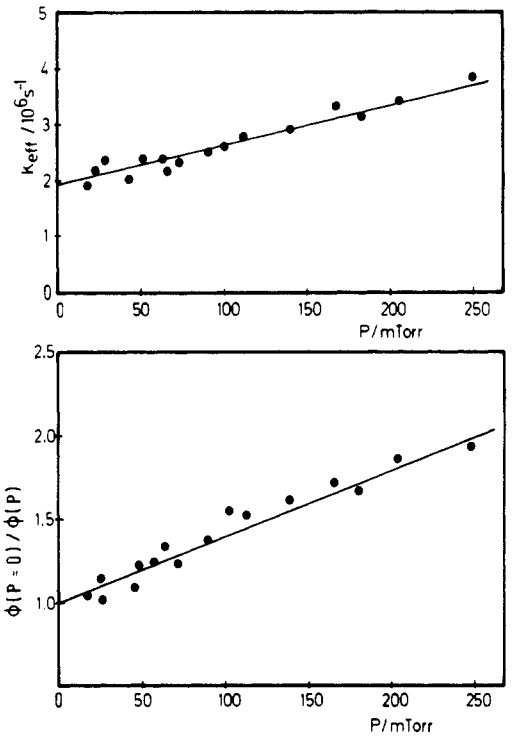

Figure 6. First-order rate coefficient k_{eff} of benzyl formation and Stern–Volmer plot of benzyl yield in the dissociation of toluene (P = toluene pressure; photolysis wavelength = 193.3 nm).

pressures of 18 and 120 mTorr in the absence of added N_2. There is an initial absorption step due to the excitation of toluene. It is difficult to identify these steps in the figures, but they can be reconstructed with the absorption coefficients of hot toluene and of hot benzyl. Figure 4 shows the absorption rise described by eq 1. With the higher pressures of Figure 5, the cooling of the spectrum sets in and becomes apparent after about 2 μs. The pressure dependence of the apparent rate coefficient $k_{eff}(P)$ is illustrated in Figure 6. Extrapolation to zero pressure gives $k(E_{ac}) = (1.9 \pm 0.2) \times 10^6$ s^{-1} for $E_{ac} = 52730$ cm^{-1} (with a thermal energy corresponding to 990 cm^{-1} at 300 K). The slope of Figure 6, with a Lennard-Jones collision frequency of $Z_{LJ} = 2.45 \times 10^7$ Torr^{-1} s^{-1}, leads to a collision efficiency $\gamma_c = 0.30$. This value is in good agreement with estimates based on energy-transfer data from ref 19 and the treatment for γ_c of ref 21. The pressure dependence of the product yields, such as also shown in Figure 6, corresponds completely to that of $k_{eff}(P)$.

On the basis of the absorption coefficients of hot toluene and benzyl such as given above, a primary benzyl yield of about 0.75 ± 0.2 is derived, indicating dominant C–H bond split. The yield of the competing C–C bond split has to be determined by direct detection of the methyl fragment such as done in part 2.[8]

4.3. p-, m-, and o-Xylene. Figure 7 shows the pressure dependences of the apparent rate coefficients $k_{eff}(P)$ and the quantum yields $\phi(P \rightarrow 0)/\phi(P)$ for the dissociation of *p*-xylene after 193-nm excitation. Extrapolation to zero pressure gives $k(E_{ac}) = (2.7 \pm$

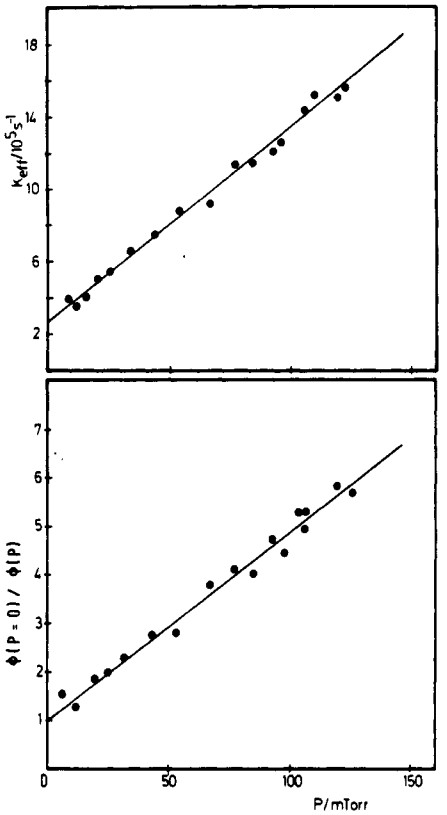

Figure 7. First-order rate coefficients and yields of product formation in the photolysis of *p*-xylene at 193.3 nm (P = *p*-xylene pressure).

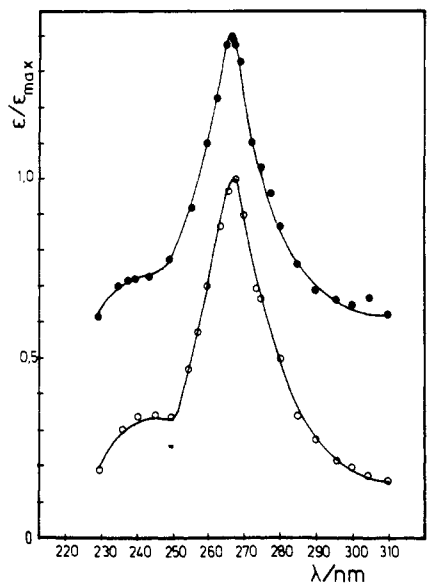

Figure 8. Product spectra from the photolysis of *p*-xylene (●) and *p*-xylyl bromide (○) (photolysis at 193.3 nm, corresponding to fragment temperatures of about 1400 K (●) and 1700 K (○); upper curve displaced vertically).

0.3) × 10^5 s^{-1} at E_{ac} = 53 070 cm^{-1} (with a room temperature thermal contribution of 1330 cm^{-1}) and a collision efficiency γ_c = 0.41 ± 0.02. Figure 8 compares the hot spectrum of the dissociation product of *p*-xylene dissociation with the hot spectrum of *p*-xylyl radicals recorded after the 193-nm photolysis of *p*-xylyl bromide. The spectra are clearly identical. They correspond to an internal temperature of (1550 ± 150) K and a maximum absorption coefficient of 7600 L mol^{-1} cm^{-1} at 266 nm and this temperature, if by analogy to benzyl chloride photolysis[25] one assumes a quantum yield of 0.9 for *p*-xylyl bromide photolysis

(25) Ichimura, T.; Mori, Y. *J. Chem. Phys.* **1972**, *57*, 1677.

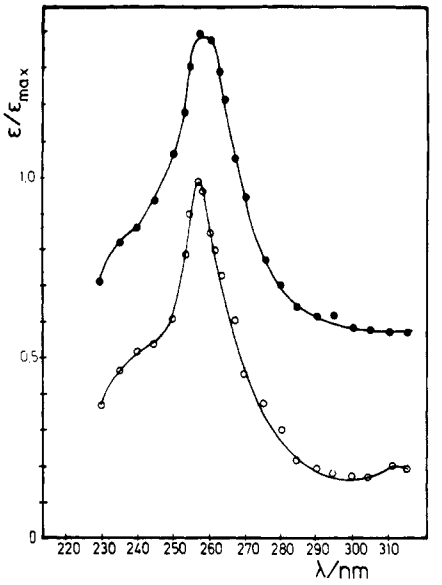

Figure 9. Product spectra from the photolysis of *m*-xylene (●) and *m*-xylyl bromide (○) at 193.3 nm (as Figure 12, T = 1550 ± 150 K).

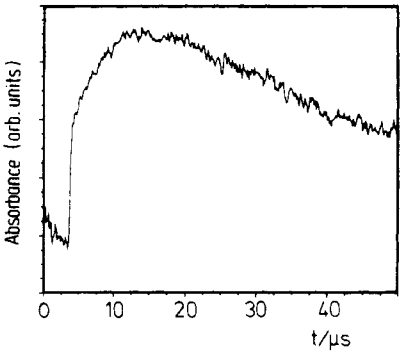

Figure 10. Absorption-time profile of product formation during the dissociation of mesitylene at 193.3 nm (detection at 266 nm; mesitylene pressure = 11.2 mTorr).

to *p*-xylyl radicals. From the final absorption levels after *p*-xylene dissociation, a yield of *p*-xylyl (= 4-methylbenzyl) radicals of about 75% is estimated. C-H bond split in one of the methyl groups thus is the dominant dissociation pathway.

The results for *o*- and *m*-xylene are similar to those of *p*-xylene. Representations of $k_{eff}(P)$ and $\phi(P\rightarrow 0)/\phi(P)$ look quite similar to Figure 7 and are not given here. The results are $k(E_{ac})$ = (3.9 ± 0.4) × 10^5 s^{-1} and $k(E_{ac})$ = (3.4 ± 0.3) × 10^5 s^{-1} at E_{ac} = 53 130 and 53 065 cm^{-1} for *o*- and *m*-xylene, respectively. The measured collision efficiencies are γ_c = 0.43 ± 0.02 and 0.39 ± 0.02. The product spectra of *o*- and *m*-xylene dissociation are identical and agree with the spectra from *o*- and *m*-xylyl bromide photolysis at 193 nm such as demonstrated in Figure 9 for *m*-xylene. A maximum absorption coefficient 6500 L mol^{-1} cm^{-1} at 257 nm for (1550 ± 150) K was obtained, as before assuming a quantum yield of 0.9 for the bromide photolysis. Since the absorption maximum for *p*-xylyl is located at 268 nm (ϵ = 7600 L mol^{-1} cm^{-1}), a fast isomerization between the ortho and meta isomers is not excluded whereas the para isomer does not appear to isomerize before the dissociation. The dominant dissociation pathways again are C-H bond splits in the methyl groups with estimated yields near 90% and 80% for *o*- and *m*-xylene, respectively.

4.4. Mesitylene. Mesitylene dissociates more slowly than the xylenes such that cooling of the spectrum was superimposed on the fragment formation signals in the applied pressure range. Figure 10 demonstrates this behavior. A deconvolution of the signal was easily achieved since the cooling behavior was well-defined. Figure 11 shows $k_{eff}(P)$ vs P, leading to $k(E_{ac})$ = (1.3 ± 0.1) × 10^5 s^{-1} at E_{ac} = 53 380 cm^{-1} and γ_c = 0.54 ± 0.04. The fragment spectrum in this case was not used for product identi-

TABLE I: Experimental Values of Specific Rate Constants $k(E_{ac})$ for C–H and C–C Bond Splits in Alkylbenzenes

reactant	fragment	$\langle E_{ac}/cm^{-1}\rangle$	$k(E_{ac})/s^{-1}$	press./mTorr	ref
		C–H Bond Splits			
toluene (from CHT)	benzyl	52080	$(3 \pm 1.5) \times 10^6$	40	4
toluene	benzyl	52730	$(2.4 \pm 0.2) \times 10^6$	10–50	5
toluene	benzyl	52730	$(2.01 \pm 0.04) \times 10^6$	10–100	10
toluene (from CHT)	H	52080	$(2.6 \pm 0.5) \times 10^6$	1–5	6
toluene	H	52730	$(3 \pm 0.5) \times 10^6$	1–5	6
toluene	benzyl	52730	$(1.9 \pm 0.2) \times 10^6$	0 (20–250)	this work
p-xylene	H	53070	$(8 \pm 3) \times 10^5$	1–5	6
p-xylene	H	53070	3.6×10^5	1–5	11
p-xylene	*p*-xylyl	53070	$(2.7 \pm 0.3) \times 10^5$	0 (10–120)	this work
m-xylene	H	53065	3.8×10^5		11
m-xylene	*m*-xylyl	53065	$(3.4 \pm 0.3) \times 10^5$	0 (5–70)	this work
o-xylene	H	53130	3.2×10^5	1–5	11
o-xylene	*o*-xylyl	53130	$(3.9 \pm 0.4) \times 10^5$	0 (2–70)	this work
mesitylene	H	53380	1.4×10^5	1–5	11
mesitylene	mesitylyl	53380	$(1.3 \pm 0.1) \times 10^5$	0 (1–15)	this work
		C–C Bond Splits			
ethylbenzene	benzyl	52960	2×10^7	10–50	5
ethylbenzene	benzyl	52960	$(2.55 \pm 0.03) \times 10^7$	10–100	10
ethylbenzene	benzyl	52960	$(2.3 \pm 0.2) \times 10^7$	0 (20–350)	this work
n-propylbenzene	benzyl	53290	6.6×10^6	10–50	5
isopropylbenzene	phenylethyl	53290	$(1.0 \pm 0.1) \times 10^7$	0 (30–600)	this work
n-butylbenzene	benzyl	53580	$(1.62 \pm 0.05) \times 10^6$	10–100	10
tert-butylbenzene	[phenylpropyl]	53580	$(2.0 \pm 0.4) \times 10^6$	0 (50–450)	this work

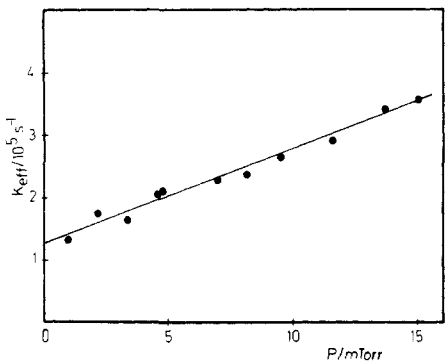

Figure 11. First-order rate coefficients of k_{eff} of product formation in the dissociation of mesitylene (P = mesitylene pressure; photolysis wavelength = 193.3 nm).

fication and yield measurement since a sufficient signal-to-noise ratio was only attainable at mesitylene pressures where collisional quenching was becoming important. However, the observed reduction of $k(E_{ac})$ in comparison to the xylenes and to toluene strongly suggests that the C–H bond split, leading to 3,5-dimethylbenzyl radicals, again is the dominant reaction pathway. The C–H bond energies in toluene, xylene, and mesitylene are nearly equal,[26,27] being close to 30000 cm^{-1} (see below).

4.5. Isopropylbenzene. The C–C bond split in ethylbenzene occurred more quickly than the C–H bond split in the isomeric xylenes. Similarly, a much faster dissociation rate was found in isopropylbenzene dissociation than in mesitylene. From the pressure dependence of $k_{eff}(P)$ we obtained $k(E_{ac}) = (1.0 \pm 0.1) \times 10^7\ s^{-1}$ at $E_{ac} = 53290\ cm^{-1}$ and $\gamma_c = 0.36 \pm 0.04$. The value of $k(E_{ac})$ suggests a C–C bond split in this case. In order to identify the fragment radical, as for ethylbenzene we cooled the product spectrum by the addition of 6 Torr of N_2. We compared the resulting 300 K spectrum with that from the 193-nm photolysis of 1-phenylethyl bromide. Figure 12 demonstrates the complete agreement between the two spectra. The time-dependent cooling profiles of the spectra were also identical in the two cases such that a dominant dissociation of isopropylbenzene to 1-phenylethyl and CH_3 is well established. A yield of >80% is estimated from the absorption coefficients. At the maximum of 244 nm, an absorption coefficient of 24000 L mol^{-1} cm^{-1} was estimated for the room temperature spectrum of 1-phenylethyl.

4.6. tert-Butylbenzene. The pressure dependence of $k_{eff}(P)$ for 193-nm dissociation of *tert*-butylbenzene was characterized by $k(E_{ac}) = (2.0 \pm 0.4) \times 10^6\ s^{-1}$ at $E_{ac} = 53580\ cm^{-1}$ and $\gamma_c = 0.34 \pm 0.02$. The observed rate coefficient, in comparison to the other substances, again clearly suggests a dominant C–C bond split and rules out a C–H bond split. Suitable precursors for the expected 2-phenylisopropyl fragment radicals were not available. The photochemistry of such substances has not been studied before. Therefore, we could not directly identify the product.

VLPP experiments for *tert*-butylbenzene at temperatures up to 1100 K have shown that 2-phenylisopropyl is the dominant dissociation product under these conditions. At 1100 K, the average energy is 40000 cm^{-1}, such that other reaction channels have to be discussed for the higher energies of the present dissociation (53580 cm^{-1}). Such processes are the elimination reaction to α-methylstyrene and methane or the dissociation to phenyl and *tert*-butyl. The fragment observed here from the 193-nm dissociation of *tert*-butylbenzene had a hot absorption coefficient of about 75000 L mol^{-1} cm^{-1} at 266 nm. This value greatly exceeds the hot absorption coefficients of α-methylstyrene[3] and phenyl[29] radicals at 266 nm, being of the order of 1500 and 1800 L mol^{-1} cm^{-1}. For this reason, the dominant channel (>80%) also at the present excitation energy has to be the C–C bond split leading to 2-phenylisopropyl radicals.

4.7. Multiphoton Excitation. It should be emphasized that the present results correspond to single UV proton excitation

(26) Benson, S. W. *Thermochemical Kinetics*, 2nd ed.; Wiley: New York, 1976.
(27) Hayashibara, K.; Krupa, G. H.; Beauchamp, J. C. *J. Am. Chem. Soc.* **1986**, *198*, 5441.
(28) Robaugh, D. A.; Stein, S. E. *Int. J. Chem. Kinet.* **1981**, *13*, 445.
(29) Ikeda, N.; Nakashima, N.; Yoshihara, K. *J. Am. Chem. Soc.* **1985**, *107*, 3318.

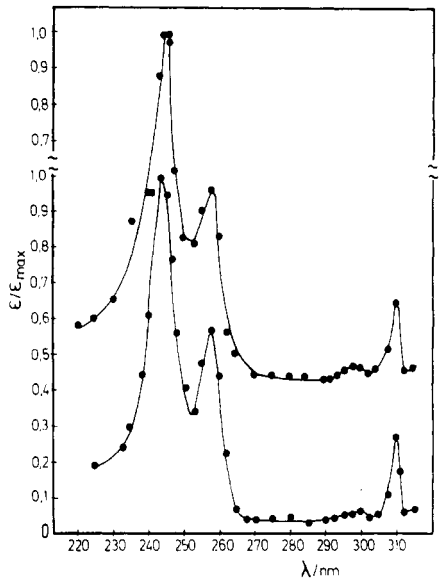

Figure 12. Absorption spectra of the products of the photolysis at 193.3 nm of isopropylbenzene (upper curve) and of 1-phenylethyl bromide (lower curve) after cooling of the radicals by 6 Torr of N_2 to T = 300 K.

conditions. Our separate experiments in part 3[16] show that the present laser energies were all in a range where less than 5% of the two-photon excitations occurred. Adding about 100 mTorr of N_2 which, e.g., in toluene dissociation, would have quenched the single-photon reaction, did not lead to appreciable absorption signals from products.

5. Discussion

5.1. Comparison of Measured k(E). Table I summarizes the present results and compares the measured specific rate constants with the data from refs 4–6, 10, and 11. The investigated dissociations obviously fall into two groups. The series toluene, all xylenes, and mesitylene is dominated by C–H bond split in the alkyl substituents. The series ethyl-, isopropyl-, and *tert*-butylbenzene dissociates via C–C bond split in the alkyl substituents. With 193-nm excitation, the latter group is characterized by markedly faster dissociation rates than the isomers in the first group. This effect is rationalized in the theoretical analysis given in the following.

The agreement between the various studies is quite good and within the experimental uncertainties. In some cases (in ref 10) a pressure dependence of $k_{eff}(P)$ was not noticed, although there is clearly some dependence such as shown in the present work. Also, some unrecognized two-photon contribution to the signals may have been present in the earlier work. Finally, the fast loss of hydrogen atoms from the observation volume at low pressures had to be corrected for in refs 6 and 11 which may have influenced the accuracy of the measurements of the slowest rates. Nevertheless, the reliability of the data appears highly sufficient for a conversion of the laser excitation into thermal excitation results such as given below.

5.2. SACM Calculations of Specific Rate Constants k(E,J) and of Thermally Averaged Rate Constants for Dissociation and Recombination. The measured "specific" rate constants $k(E_{ac})$ from the present type of experiments are not completely specific in the sense that no averaging over energy E and angular momentum J would be involved. Instead, the excitation process is believed to carry the room temperature thermal vibrational and rotational distribution together with the photon up into the excited state. For this reason, we calculate specific rate constants $k(E,J)$ by the statistical adiabatic channel model (SACM) of refs 30–33

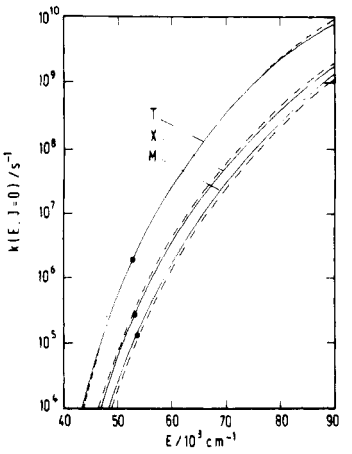

Figure 13. Specific rate constants $k(E,J=0)$ for C–H bond splits in toluene (T), *o*-xylene (X), and mesitylene (M) (SACM calculations reproducing the measured k_{eff} of this work; dashed lines, $k(E,J)$ = 100).

in a way such that $k(E_{ac})$ is reproduced. The modeling leads to complete sets of $k(E,J)$ curves which will be illustrated and discussed in the following. Afterwards, thermal averaging of $k(E,J)$ is performed for room temperature photolysis as well as for thermal dissociation and recombination conditions. In this way thermal dissociation and recombination rate constants, $k_{diss,\infty}$ and $k_{rec,\infty}$ respectively, are obtained which are consistent with the laser excitation results.

The modeling procedure is not without problems. At present, it is based on the simplified SACM treatment proposed in refs 31–33. It is a single-fit-parameter version of the theory[34] which so far generally was sufficient for experimental applications. More detailed eigenvalue and potential energy surface treatments[35–37] ultimately, however, will have to be applied. At present these detailed versions are not yet available for molecules of the size of the aromatics studied here. Unfortunately, the simplified SACM may not be free from artifacts. Our treatment in ref 2 showed that, at values of the anisotropy ratio α/β near 0.5, too small values of $k_{diss,\infty}$ arise (see Figure 13 in ref 2). The reason for this behavior is the use of the empirical relationship ((3.22) from ref 31) between the quanta ϵ of the disappearing oscillators and the ratio α/β for a case with a very small product rotational constant. In this case one goes beyond the range for which the relationship $\epsilon(\alpha/\beta)$ (also $x(\alpha/\beta)$ in ref 31) was derived. In order to correct for this artifact, in the present work we fixed the ratio α/β to the standard value of 0.5 from ref 33. We then multiplied the results with an empirical temperature- and energy-independent correction factor such that the most certain experimental values, either $k(E_{ac})$ or $k_{diss,\infty}$ or $k_{rec,\infty}$, were reproduced. There is an additional complication: the values of the bond energies are often not known sufficiently precisely and had to be adjusted slightly as well. Our recent work[38] analyzing dissociation equilibria involving benzyl radicals, e.g., had to slightly modify the enthalpy of formation of benzyl which also influences the bond energies of toluene and ethylbenzene. Since the bond energies of the xylenes and of mesitylene have been measured relative to the bond energies of toluene and ethylbenzene,[27,39] the bond energies of the other molecules studied here also had to be modified. We shall demonstrate in the following how, in spite of these minor uncertainties of the modeling procedure and the input molecular data, a general picture of convincing internal consistency arises.

5.3. Calculations for C–H Bond Splits in Toluene, Xylenes, and Mesitylene. Toluene. Our SACM calculations employed the molecular parameters for toluene and benzyl given in ref 2.

(30) Quack, M.; Troe, J. *Ber. Bunsen-Ges. Phys. Chem.* **1974**, *78*, 240.
(31) Troe, J. *J. Chem. Phys.* **1981**, *75*, 266.
(32) Brouwer, L.; Cobos, C. J.; Troe, J.; Dübal, H.-R.; Crim, F. F. *J. Chem. Phys.* **1987**, *86*, 6171.
(33) Cobos, C. J.; Troe, J. *J. Chem. Phys.* **1985**, *83*, 1010.
(34) Troe, J. *Ber. Bunsen-Ges. Phys. Chem.* **1988**, *92*, 242.
(35) Troe, J. *J. Phys. Chem.* **1986**, *90*, 3485.
(36) Troe, J. *J. Chem. Phys.* **1987**, *87*, 2773.
(37) Troe, J. *Z. Phys. Chem. (Frankfurt)* **1989**, *161*, 209.
(38) Hippler, H.; Troe, J. *J. Phys. Chem.* **1990**, *94*, 3803.
(39) Barton, B. D.; Stein, S. E. *J. Phys. Chem.* **1980**, *84*, 2141.

TABLE II: SACM Calculations of Specific Rate Constants $k(E,J)$ for C–H and C–C Bond Splits[a]

			$k(E,J)/s^{-1}$							
			E/cm^{-1} =							
molecule	$E_0(J)/cm^{-1}$	J	45000	50000	55000	60000	70000	80000	90000	100000
toluene	31 080	0	3.2×10^4	5.4×10^5	4.7×10^6	2.6×10^7	3.5×10^8	2.2×10^9	8.3×10^9	2.3×10^{10}
	31 640	100	3.1×10^4	5.0×10^5	4.6×10^6	2.7×10^7	3.6×10^8	2.2×10^9	8.8×10^9	2.5×10^{10}
m-xylene	[30 000]	0	4.5×10^3	8.2×10^4	7.6×10^5	4.6×10^6	7.0×10^7	5.0×10^8	2.2×10^9	7.2×10^9
	[30 400]	100	4.3×10^3	8.0×10^4	7.7×10^5	4.7×10^6	7.3×10^7	5.3×10^8	2.4×10^9	7.6×10^9
	[30 950]	0	3.7×10^3	7.7×10^4	8.5×10^5	5.6×10^6	9.4×10^7	7.5×10^8	3.6×10^9	1.2×10^{10}
	[31 350]	100	3.0×10^3	7.1×10^4	7.9×10^5	5.4×10^6	9.7×10^7	7.8×10^8	3.7×10^9	1.3×10^{10}
p-xylene	[30 000]	0	3.7×10^3	6.5×10^4	6.0×10^5	3.6×10^6	5.3×10^7	3.8×10^8	1.7×10^9	5.3×10^9
	[30 350]	100	3.9×10^3	7.2×10^4	6.7×10^5	4.1×10^6	6.1×10^7	4.3×10^8	1.9×10^9	6.0×10^9
	[30 950]	0	2.8×10^3	5.9×10^4	6.3×10^5	4.2×10^6	7.2×10^7	5.6×10^8	2.7×10^9	9.0×10^9
	[31 300]	100	2.9×10^3	6.5×10^4	7.0×10^5	4.7×10^6	8.2×10^7	6.4×10^8	3.0×10^9	1.0×10^{10}
o-xylene	[30 000]	0	5.0×10^3	9.0×10^4	8.4×10^5	5.1×10^6	7.9×10^7	5.7×10^8	2.6×10^9	8.3×10^9
	[30 680]	100	3.1×10^3	6.3×10^4	6.3×10^5	4.0×10^6	6.6×10^7	4.9×10^8	2.3×10^9	7.4×10^9
	[30 760]	0	3.9×10^3	8.4×10^4	8.8×10^5	5.8×10^6	1.0×10^8	7.9×10^8	3.8×10^9	1.3×10^{10}
	[31 440]	100	2.4×10^3	5.7×10^4	6.5×10^5	4.5×10^6	8.3×10^7	6.7×10^8	3.3×10^9	1.1×10^{10}
mesitylene	[29 200]	0	1.3×10^3	2.5×10^4	2.6×10^5	1.7×10^6	3.2×10^7	2.5×10^8	1.3×10^9	4.5×10^9
	[29 710]	100	9.0×10^2	1.9×10^4	2.1×10^5	1.4×10^6	2.6×10^7	2.2×10^8	1.1×10^9	4.1×10^9
	[30 000]	0	1.0×10^3	2.3×10^4	2.7×10^5	1.9×10^6	3.9×10^7	3.6×10^8	1.9×10^9	7.2×10^9
	[30 510]	100	6.8×10^2	1.7×10^5	2.1×10^5	1.6×10^6	3.4×10^7	3.2×10^8	1.7×10^9	6.5×10^9

			$k(E,J)/s^{-1}$							
			E/cm^{-1} =							
molecule	$E_0(J)/cm^{-1}$	J	40000	45000	50000	55000	60000	70000	80000	90000
ethylbenzene	26 910	0	5.0×10^4	9.3×10^5	8.1×10^6	4.4×10^7	1.7×10^8	1.4×10^9	6.3×10^9	1.9×10^{10}
	27 120	100	6.1×10^4	1.1×10^6	9.8×10^6	5.3×10^7	2.0×10^8	1.7×10^9	7.4×10^9	2.2×10^{10}
isopropylbenzene	[25 820]	0	1.8×10^4	3.3×10^5	3.0×10^6	1.7×10^7	6.9×10^7	5.9×10^8	2.7×10^9	8.6×10^9
	[26 000]	100	2.0×10^4	3.8×10^5	3.5×10^6	2.0×10^7	7.9×10^7	6.6×10^8	3.0×10^9	9.5×10^9
tert-butylbenzene	[24 510]	0	4.4×10^3	7.0×10^4	5.8×10^5	3.1×10^6	1.2×10^7	9.5×10^7	4.3×10^8	1.3×10^9
	[24 750]	100	4.9×10^3	7.9×10^4	6.6×10^5	3.5×10^6	1.3×10^7	1.1×10^8	4.7×10^8	1.5×10^9

[a] Molecular parameters from ref 13; $\alpha/\beta = 0.5$; results scaled to reproduce measured $k(E_{ac})$; [ ]: uncertain E_0 values, see text.

They were used without change except for the new value[38] of the toluene bond energy (increased by 900 cm^{-1}). An all-vibrational model for benzyl was used as in ref 38 with a frequency of 290 cm^{-1} for CH_2 torsion against the phenyl ring. The modeled $k(E,J)$ were scaled with an energy-independent empirical correction factor of 2.7 such that the measured $k(E_{ac}=52730\ cm^{-1}) = 1.9 \times 10^6$ s^{-1} was reproduced. The corresponding modeled $k(E,J)$ values in Table II are given for $J = 0$ and 100. They are illustrated in Figure 13.

While the modeled $k(E,J)$ curves are forced to coincide with the measured $k(E_{ac})$ from the present laser photolysis experiments (by multiplication with an empirical correction factor 2.7), no further adjustments are made in calculating thermally averaged dissociation and recombination rate constants $k_{diss,\infty}$ and $k_{rec,\infty}$. Table III compares these calculated values with the most recent experimental data.[40-43] There is excellent agreement in the absolute values, although the apparent activation energy of the experimental expression for $k_{diss,\infty}$ is somewhat low. This in part is due to the neglect of falloff effects at the highest temperatures. The experimentally observed independence of $k_{rec,\infty}$ on the temperature is reproduced well by the calculation. One should note that the temperature coefficient of $k_{rec,\infty}$ sensitively depends on the ratio α/β and that the choice of $\alpha/\beta = 0.5$ is consistent with a temperature-independent $k_{rec,\infty}$.

p-Xylene. The analysis of $k(E_{ac})$ for dissociation of *p*-xylene is less straightforward than that for toluene since less direct information on the C–H bond energy is available. Also thermal dissociation[44-46] and recombination[47] experiments are more fragmentary. The dissociation energy has been discussed in ref 39 where the pyrolysis of methyl-substituted ethylbenzenes was measured and evaluated assuming equal A factors as in ethylbenzene. Alternatively, photoelectron spectroscopy of *p*-methylbenzyl in ref 27 relates the C–H bond energy in *p*-xylene to that in toluene. However, a number of assumptions about auxiliary quantities had to be made. Although both sources agree that the C–H bond energy in xylene is slightly lower than in toluene (by[39] (1.3–1.7) ± 7 kJ mol^{-1} or[27] 2.47 ± 2 kJ mol^{-1}), there appears to be some uncertainty with regard to the exact difference. We, therefore, allowed for an adjustment of the C–H bond energy in order to obtain a similar consistency as in toluene. SACM calculations employed the molecular parameters given in ref 13. An empirical correction factor of 2.7 was applied to obtain agreement with the measured[47] $k_{rec,\infty}$, since this value is independent of the uncertainty in the bond energy E_0. The E_0 value then was adjusted in order to bring the calculated $k(E_{ac})$ in agreement with the laser photolysis measurement. Simultaneously, agreement with the measured absolute value[44-46] of $k_{diss,\infty}$ was obtained whereas the apparent activation energies of the measurements turned out to be too low such as was observed for toluene. The resulting specific rate constants $k(E,J)$ are included in Table II and Figure 13 whereas the thermal dissociation and recombination results are given in Table III. The fitted C–H bond energy of 359 kJ mol^{-1} (at 0 K) is 13 kJ mol^{-1} lower than the bond energy in toluene. We, therefore, deduce a larger difference in C–H bond energies than derived in refs 27 and 39. However, more systematic studies of thermal dissociation and recombination such as for toluene[38] would be required to verify this observation. The effect of changing the bond energy E_0 on the fitted values is also included in Table III (by the values in parentheses) such that later improvements in the thermochemistry could be taken into account.

o- and m-Xylene. For these molecules the data are even more fragmentary, since only few studies on thermal dissociation[44,46] but no recombination experiments are available. The C–H bond energy appears to be similar in *p*- and *m*-xylene whereas for *o*-xylene it is supposed to be 4 kJ mol^{-1} below the C–H bond energy

(40) Ackermann, L.; Hippler, H.; Pagsberg, P.; Troe, J. *J. Phys. Chem.*, in press. Bartels, M.; Edelbüttel-Einhaus, J.; Hoyermann, K. H. *Proceedings of the 22nd International Symposium on Combustion*; The Combustion Institute: Pittsburgh, 1988; p 1041.
(41) Hippler, H.; Reihs, C.; Troe, J. *Z. Phys. Chem. (Frankfurt)*, in press.
(42) Price, S. J. *Can. J. Chem.* **1962**, *40*, 1310.
(43) Braun-Unkhoff, M.; Frank, P.; Just, Th. To be published.
(44) Brouwer, L. D. Ph.D. Dissertation, Göttingen, 1984. Brouwer, L.; Müller-Markgraf, W.; Troe, J. *Proceedings of the 20th International Symposium on Combustion*; The Combustion Institute: Pittsburgh, 1984; p 799.
(45) Swarc, M. *J. Chem. Phys.* **1948**, *16*, 128.
(46) Errede, L. A.; DeMaria, F. *J. Phys. Chem.* **1962**, *66*, 2664.
(47) Ackermann, L. Ph.D. Dissertation, Göttingen, 1982.

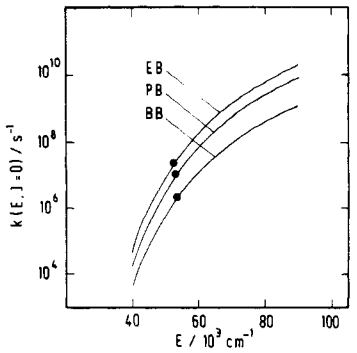

Figure 14. As Figure 13, for the C–C bond splits in ethylbenzene (EB), isopropylbenzene (PB), and *tert*-butylbenzene (BB).

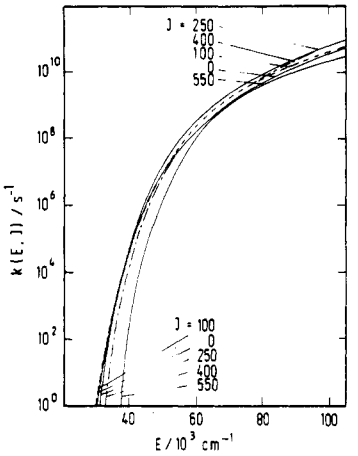

Figure 15. Specific rate constants $k(E,J)$ for the C–c bond split in ethylbenzene (SACM calculations reproducing the measured k_{eff} of this work).

in toluene.[27,39] Our SACM calculations used the parameters given in ref 13. Correction factors of 2.2 (*o*-xylene) and 2.0 (*m*-xylene) were applied and E_0 was adjusted to E_0 = 359 kJ mol^{-1} in order to arrive at an optimum fit with the measured specific rate constants $k(E_{ac})$ and recombination rate coefficients close to $k_{rec,\infty}$ = 10^{14} cm^3 mol^{-1} s^{-1} such as measured for H + benzyl, H + *p*-methylbenzyl or H – cyclohexadienyl.[41] Simultaneously a prediction of $k_{diss,\infty}$ is obtained which is consistent with the value of $k(E_{ac})$ and which can be compared with earlier measurements near 110 K. Tables II and III give the derived specific and thermally averaged rate constants.

Mesitylene. The studies of mesitylene (1,3,5-trimethylbenzene) dissociation are even less complete than for *m*- and *o*-xylene. The discussion from ref 39, in combination with our new toluene dissociation energy, leads to a C–H bond energy of 337 ± 7 kJ mol^{-1} (at 0 K). Adjusting our SACM calculation by a correction factor of 2.4 and choosing a bond energy of $\Delta H°_0$ = 349 kJ mol^{-1}, we obtain agreement with the measurements of $k(E_{ac})$ and a "reasonable" value of $k_{rec,\infty}$. The results from our calculations are included in Tables II–IV and Figure 13. Changes in E_0 can be taken into account with the values in parentheses in Table III.

5.4. Calculations for C–C Bond Splits in Ethylbenzene, Isopropylbenzene, and tert-Butylbenzene. Ethylbenzene. For this system, the new bond energy from ref 38 was used which appears to be well established. Our SACM calculations of $k(E,J)$ with α/β = 0.5 were scaled with an energy-independent correction factor of 0.68 such that the measured $k(E_{ac})$ was reproduced. Figures 14 and 15 demonstrate the E and J dependences of $k(E,J)$ over wide ranges of conditions. After thermal averaging of these $k(E,J)$, the values given in Table III are obtained. They agree very well with experimental results for the dissociation reaction over a wide temperature range.[3,28,48-59] Our calculations produce

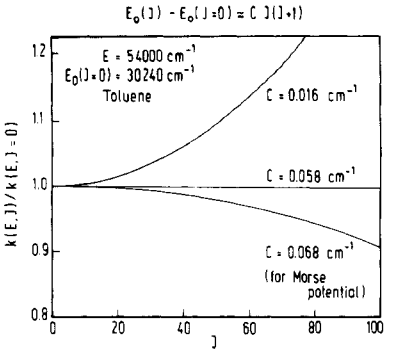

Figure 16. Angular momentum (J) dependence of specific rate constants $k(E,J)$ for toluene dissociation at E = 54000 cm^{-1} (SACM calculations with centrifugal barriers of the type $E_0(J) - E_0(J=0) = CJ(J+1)$ and Morse potential, see text. Realistic value: C = 0.058 cm^{-1}).

a somewhat higher apparent activation energy than obtained from individual sets of most experimental data. However, some unidentified falloff effects may have been present in the high-temperature experiments. Also, via H atom production at high temperatures, the ethylbenzene and toluene dissociation systems are intimately coupled such that some mechanistic complications still may not have been ruled out in the experiments. The controversy about dominant C–H or C–C bond splits in ethylbenzene[48,53] appears to be solved now[2] in favor of a C–C bond split. This situation may, nevertheless, change with higher excitation energies, see parts 2[8] and 3.[16] Compared to the C–H bond splits discussed in section 5.3 the near coincidence of the preexponential factors of $k_{diss,\infty}$ of C–C bond splits should be noted. However, the recombination rate constants for the addition of H atoms to the radicals of section 5.3 are about an order of magnitude higher than for the recombination of methyl with benzyl.

Isopropylbenzene. Our analysis of the experimental data for this system has encountered difficulties. There is, at first, the uncertainty of the bond energy which we cannot resolve before measurements of the reverse recombination are also available. Fitting our SACM calculations of $k(E,J)$ with α/β = 0.5 to the experimental value of $k(E_{ac})$ requires a correction factor of 1.9. With this value, recombination rate constants of (1–2) × 10^{13} cm^3 mol^{-1} s^{-1} are obtained. Whereas no experimental values of recombination rate constants are available for a comparison, the calculated dissociation rate constants are all about a factor of 3–4 higher than the measurements (except for the single experiment from ref 44 which may have been contaminated by secondary reactions). On the other hand, the measured value of $k(E_{ac})$ appears to be 2–3 times higher compared to ethylbenzene, *n*-propylbenzene, *n*-butylbenzene, and *tert*-butylbenzene. We have reinspected our laser experiments and found no evidence for any particular perturbation. It should be noted that a change in E_0, such as demonstrated for the xylenes or mesitylene, does not bring $k_{diss,\infty}$ and $k(E_{ac})$ values into better agreement. Therefore, we are

(48) Robaugh, D. A.; Tsang, W.; Fahr, A.; Stein, S. E. *Ber. Bunsen-Ges. Phys. Chem.* **1986**, *90*, 77.
(49) Swarc, M. J. *J. Chem. Phys.* **1949**, *17*, 431.
(50) Crowne, C. W. P.; Grigulis, V. J.; Thorssell, J. J. *Trans. Faraday Soc.* **1969**, *65*, 1051.
(51) Clarke, W. D.; Price, S. J. *Can. J. Chem.* **1970**, *48*, 1059.
(52) Esteban, G. L.; Kerr, J. A.; Trotman-Dickenson, A. F. *J. Chem. Soc.* **1963**, 3873.
(53) Brouwer, L.; Müller-Markgraf, W.; Troe, J. *Ber. Bunsen-Ges. Phys. Chem.* **1983**, *87*, 1031.
(54) McMillen, D. F.; Trevor, P. L.; Golden, D. M. *J. Am. Chem. Soc.* **1980**, *102*, 740.
(55) Davis, H. G. *Int. J. Chem. Kinet.* **1983**, *15*, 469.
(56) Mizerka, L. J.; Kiefer, J. H. *Int. J. Chem. Kinet.* **1986**, *18*, 363.
(57) Rao, V. S.; Skinner, G. B. *Symp. (Int.) Combust., (Proc.), 21st* **1986**, 809.
(58) Pamidimukkala, K. M.; Kern, R. D. *Int. J. Chem. Kinet.* **1986**, *18*, 1341.
(59) Gonzalez, A. C.; Larson, C. W.; McMillen, D. F.; Golden, D. M. *An. Asoc. Quim. Argent.* **1985**, *73*, 141.
(60) Leigh, C. H.; Swarc, M. *J. Chem. Phys.* **1952**, *20*, 844.
(61) Kerr, J. A.; Trotman-Dickenson, A. F.; Wolter, M. *J. Chem. Soc.* **1964**, 3584.

TABLE III: Rate Constants $k_{diss,\infty}$ and $k_{rec,\infty}$ for Thermal Dissociation and Recombination[a]

reaction	T/K	$k_{diss,\infty}/s^{-1}$	$k_{rec,\infty}/cm^3\ mol^{-1}\ s^{-1}$	ref
toluene → benzyl + H (E_0 = 371.8 kJ mol^{-1} = 31080 cm^{-1})	300		1.8×10^{14} (SACM)	a
			$(2–3) \times 10^{14}$ (exp)	40
	1100		2.0×10^{14} (SACM)	a
	1300–1600		2×10^{14} (exp)	41
	1000	1.6×10^{-4} (SACM)		a
		1.6×10^{-4} (exp)		42
	300–1200	$10^{16.26} \exp(-384/RT)$ (SACM)		a
	1200–1500	$10^{15.0} \exp(-360/RT)$ (exp)		41
	910–1140	$10^{14.8} \exp(-356/RT)$ (exp)		42
	1400–1650	$10^{15.6} \exp(-374/RT)$ (exp)		43
m-xylene → *m*-xylyl + H [E_0 = 358.9 kJ mol^{-1} = 30000 cm^{-1} (370.2 kJ mol^{-1} = 30950 cm^{-1})]	300		1.2×10^{14} (SACM)	a, b
			$(3.3 \times 10^{14}$ (SACM))	a, b
	1100		1.4×10^{14} (SACM)	a, b
			$(3.7 \times 10^{14}$ (SACM))	a, b
	1900		1.5×10^{14} (SACM)	a, b
			$(4.1 \times 10^{14}$ (SACM))	a, b
	1100	4.8×10^{-2} (SACM)		a, b
		$(3.7 \times 10^{-2}$ (SACM))		a, b
		1.9×10^{-2} (exp)		45
	1100–1900	$10^{16.29} \exp(-371/RT)$ (SACM)		a, b
		$(10^{16.71} \exp(-382/RT)$ (SACM))		a, b
p-xylene → *p*-xylyl + H [E_0 = 358.9 kJ mol^{-1} = 30000 cm^{-1} (370.2 kJ mol^{-1} = 30950 cm^{-1})]	300		1.9×10^{14} (SACM)	a, b
			$(5.2 \times 10^{14}$ (SACM))	a, b
			1.5×10^{14} (exp)	47
	1100		2.2×10^{14} (SACM)	a, b
			$(6.0 \times 10^{14}$ (SACM))	a, b
	1900		2.5×10^{14} (SACM)	a, b
			$(6.8 \times 10^{14}$ (SACM))	a, b
	1100	5.4×10^{-2} (SACM)		a, b
		$(4.2 \times 10^{-2}$ (SACM))		a, b
		3.6×10^{-2} (exp)		45
		7.4×10^{-2} (exp)		46
	1100–1900	$10^{16.25} \exp(-369/RT)$ (SACM)		a, b
		$(10^{16.71} \exp(-381/RT)$ (SACM))		a, b
o-xylene → *o*-xylyl + H [E_0 = 358.9 kJ mol^{-1} = 30000 cm^{-1} (368.0 kJ mol^{-1} = 30760 cm^{-1})]	300		6.6×10^{13} (SACM)	a, b
			$(1.4 \times 10^{14}$ (SACM))	a, b
	1100		6.9×10^{13} (SACM)	a, b
			$(1.5 \times 10^{14}$ (SACM))	a, b
	1900		7.6×10^{13} (SACM)	a, b
			$(1.7 \times 10^{14}$ (SACM))	a, b
	1100	2.14×10^{-2} (SACM)		a, b
		$(1.7 \times 10^{-2}$ (SACM))		a, b
		6.9×10^{-2} (SACM)		45
	1100–1900	$10^{16.04} \exp(-373/RT)$ (SACM)		a, b
		$(10^{16.38} \exp(-382/RT)$ (SACM))		a, b
mesitylene → mesitylyl + H [E_0 = 349.3 kJ mol^{-1} = 29200 cm^{-1} (358.9 kJ mol^{-1} = 30000 cm^{-1})]	300		6.2×10^{13} (SACM)	a, b
			$(1.4 \times 10^{14}$ (SACM))	a, b
	1100		7.0×10^{13} (SACM)	a, b
			$(1.6 \times 10^{14}$ (SACM))	a, b
	1900		7.8×10^{13} (SACM)	a, b
			$(1.8 \times 10^{14}$ (SACM))	a, b
	1100	1.0×10^{-1} (SACM)		a, b
		$(9.0 \times 10^{-2}$ (SACM))		a, b
	1100–1900	$10^{16.35} \exp(-365/RT)$ (SACM)		a, b
		$(10^{16.76} \exp(-375/RT)$ (SACM))		a, b
ethylbenzene → benzyl + CH_3 (E_0 = 321.9 kJ mol^{-1} = 26910 cm^{-1})	300		8.2×10^{12} (SACM)	a
	1100		1.1×10^{13} (SACM)	a
	1900		1.1×10^{13} (SACM)	a
	1100	1.1×10^{1} (SACM)		a
		7.1×10^{0} (exp)		28, 51, 54
	1500	1.3×10^{5} (SACM)		a
		1.3×10^{5} (exp)		2, 56
	900–1700	$10^{16.32} \exp(-323/RT)$ (SACM)		a
	1050–1230	$10^{15.3} \exp(-304/RT)$ (exp)		28, 54
	1250–1680	$10^{15.78} \exp(-307/RT)$ (exp)		2
isopropylbenzene → 1-phenyl-1-ethyl + CH_3 [E_0 = 308.6 kJ mol^{-1} = 25800 cm^{-1}]	300		1.2×10^{13} (SACM)	a, b
	1100		1.6×10^{13} (SACM)	a, b
	1900		1.6×10^{13} (SACM)	a, b
	900	3.1×10^{-2} (exp)		60
		1.9×10^{-2} (exp)		61
		7.9×10^{-2} (SACM)		a, b
	1100	4.3×10^{1} (exp)		28, 48
		1.6×10^{2} (SACM)		a, b

TABLE III (Continued)

reaction	T/K	$k_{diss,\infty}$/s^{-1}	$k_{rec,\infty}$/cm^3 mol^{-1} s^{-1}	ref
	1243	1.8×10^3 (exp)		48
		7.3×10^3 (SACM)		a, b
	1340	5.5×10^4 (exp)		44
		6.4×10^4 (SACM)		a, b
	970–1150	$10^{15.8}$ exp(−298/RT) (exp)		28
	900–1700	$10^{16.89}$ exp(−310/RT) (SACM)		a, b
tert-butylbenzene → 2-phenyl-2-propyl + CH_3 [E_0 = 293.1 kJ mol^{-1} = 24500 cm^{-1}]	300		6.8×10^{12} (SACM)	a, b
	1100		7.1×10^{12} (SACM)	a, b
	1700		7.1×10^{12} (SACM)	a, b
	900	1.1×10^{-1}		60
		1.3×10^{-1}		48
		3.9×10^{-1}		a, b
	1100	1.5×10^2		48
		4.5×10^2		a, b
	930–1130	$10^{15.9}$ exp(−289/RT) (exp)		48
	900–1700	$10^{16.2}$ exp(−286/RT) (SACM)		a, b

[a] (SACM): calculations from this work with $\alpha/\beta = 0.5$ scaled to fit the laser photolysis results; (exp): measured values; a = this work, b = E_0 uncertain, alternative values given for illustration; activation energies in kJ mol^{-1}, [ ]: E_0 uncertain.

at present unable to explain the discrepancy by about a factor of 3 between the thermal and photodissociation data.

tert-Butylbenzene. Our analysis of the specific rate constants for this system and the comparison with measured dissociation data unfortunately encounters the same problems as observed with the isopropylbenzene system. The SACM calculations with $\alpha/\beta = 0.5$ with the chosen E_0 lead to agreement with the measured $k(E_{ac})$ without applying a correction factor. However, the precise value of E_0 remains uncertain. The calculated dissociation rates then are again a factor of 3 higher than the few measured values. At present we have no explanation for this discrepancy. A change of E_0 would not remove the apparent inconsistency between the measured $k(E_{ac})$ and $k_{diss,\infty}$ values.

5.5. Analysis of Rotational Effects in Specific Rate Constants $k(E,J)$. The present measurements of specific rate constants $k(E_{ac})$ correspond to averages over room temperature rotational distributions. In the following, we briefly discuss which information would be obtainable if energy E and angular momentum J specific rate constants could be measured. Experiments of this type have been realized recently in the C–H bond split of benzene cations.[62] Our SACM calculations allow us to represent $k(E,J)$ as a function of J at constant E. Figure 16 shows such a plot for toluene dissociation at $E = 54000$ cm^{-1}. Depending on the properties of the centrifugal barriers $E_0(J)$ of the reaction, $k(E,J)$ can either increase or decrease with increasing J. Activated complex treatments, which do not account for the centrifugal barriers in detail, thus fail. With a Morse-potential and a simplified quasitriatomic linear model of the moment of inertia for toluene, we obtained centrifugal barriers of the form

$$E_0(J) - E_0(J=0) \approx CJ(J+1)$$

with $C = 0.054$ cm^{-1}. For this value, according to Figure 16 $k(E,J)$ almost does not depend on J. A slight decrease was observed for benzene cations,[62] dissociating with $k(E,J)$ of the order of 10^6 s^{-1}. The trend of the J dependence depends sensitively on the parameter C such as demonstrated in Figure 16. Therefore, we have carefully reinspected our moment of inertia calculations. However, a detailed treatment confirms the results from the simple quasitriatomic linear model. We have not further inspected the potential which apparently works well at the short-range interfragment distances of interest.[33] The results from ref 62 apparently confirm this suggestion even for ionic systems. We, therefore, conclude that measurements of J dependences can provide an access to centrifugal barriers and, hence, to the potential in the dissociating bond.

It should be noted that centrifugal effects enter $k(E_{ac})$ and $k_{diss,\infty}$ (or $k_{rec,\infty}$) in different ways. The latter quantities often sample the barriers in a much more sensitive way than the former observable. In this sense, measurements of $k(E_{ac})$ and $k_{diss,\infty}$ are not completely equivalent although both quantities depend on E_0 in a parallel way.

(62) Kiermeier, A.; Kühlewind, H.; Neusser, H. J.; Schlag, E. W.; Lin, S. H. *J. Chem. Phys.* **1988**, *88*, 6182.

TABLE IV: Efficiencies γ_c and Average Transferred Energies $\langle\Delta E\rangle$ for Collisional Quenching of Photodissociation[a]

reactant	$(E_{ac} - E_0)$/cm^{-1}	S^*	$-\langle\Delta E\rangle$/cm^{-1} from γ_c	eq 6	eq 7	ref 19
toluene	22550	10.4	0.30	710	780	770
o-xylene	23130	11.8	0.39	930	1200	1000
p-xylene	23070	11.2	0.43	1040	1250	1000
m-xylene	23070	11.4	0.41	1010	1250	1000
mesitylene	23780	12.2	0.54	1500	1700	1300
Et-benzene	27660	8.5	0.50	2000		1000
i-Pr-benzene	28490	9.4	0.36	1250	1700	1300
t-Bu-benzene	29080	10.1	0.34	1110	1500	

[a] See section 5.6.

5.6. Stern–Volmer Plots of Collisional Quenching of Photolysis. The observed pressure effects of the measured photolysis rate coefficients can be analyzed without problems such as shown in the following. Table IV gives the excess energies $E_{ac} - E_0$ of the laser excitation at 193 nm, the bond energies E_0, and the exponents S^* of a simplified representation of the $\langle k(E,J)\rangle_J$ curves in the form

$$\langle k(E,J)\rangle_J \propto (E - E_0)^{S^*-1} \quad (5)$$

near $E \approx E_{ac}$. The latter quantities are used in order to relate the measured collision efficiencies γ_c, describing the quenching of the dissociation, with the average energies $\langle\Delta E\rangle$ transferred per collision. Table IV compares the $\langle\Delta E\rangle$ values derived from the simple expression[21]

$$\gamma_c/(1-\gamma_c^2) \approx -\langle\Delta E\rangle S^*/(E_{ac} - E_0) \quad (6)$$

with the results from a multistep analysis[21] of the dissociation yield ϕ, i.e.

$$1 - \phi \approx \prod_{i=1}^{T}\{1 + k(E_{ac} + (i-1)\langle\Delta E\rangle)/Z_{LJ}[M]\} \quad (7)$$

where $T = (E_{ac} - E_0)/-\langle\Delta E\rangle$. $\langle\Delta E\rangle$ values from direct studies of the energy transfer in ref 19 are also included. The agreement is quite satisfactory, proving the consistency of the present analysis.

6. Conclusions

The present experiments have demonstrated the close relationship between the specific rate constants $k(E,J)$ for dissociation of laser-excited aromatic molecules after internal conversion and thermal dissociation (or recombination) rate constants $k_{diss,\infty}$ (or $k_{rec,\infty}$). The conversion from one quantity into the other was done by using a simplified version of the SACM accounting for the J dependence of $k(E,J)$ and fitting a single parameter to reproduce

the more accurate of the experimental values. In the present case, we believe that this was the laser result. A considerable simplification of the complications of high-temperature pyrolysis experiments can thus be achieved.

The agreement between the modeling of the thermal rate constants, based on the measured laser results, and the measured thermal rate constants generally was within a factor of 2. Only for isopropylbenzene and *tert*-butylbenzene were discrepancies of about a factor of 3 observed. The incomplete knowledge about the dissociation energies in some cases left some uncertainties. However, in general, the present work showed a possibility to circumvent mechanistic difficulties in thermal dissociation experiments by using the related laser photolysis measurements. It should be mentioned that the simplified SACM formalism, fixing the α/β ratio at its universal value of 0.5, in spite of the remaining artifacts of the method and the uncertainties in the potential energy surface, apparently predicted the rate constants within about a factor of 2 accuracy without parameter fitting.

Acknowledgment. Financial support of this work by the Deutsche Forschungsgemeinschaft (Sonderforschungbereich 93 "Photochemie mit Lasern") is gratefully acknowledged.

Registry No. Toluene, 108-88-3; *m*-xylene, 108-38-3; *o*-xylene, 95-47-6; *p*-xylene, 106-42-3; mesitylene, 108-67-8; ethylbenzene, 100-41-4; isopropylbenzene, 98-82-8; *tert*-butylbenzene, 98-06-6; methyl, 2229-07-4.

C–C and C–H Bond Splits of Laser-Excited Aromatic Molecules. 2. In Situ Measurements of Branching Ratios

K. Luther, J. Troe,* and K.-M. Weitzel

Institut für Physikalische Chemie der Universität Göttingen, Tammannstrasse 6, D-3400 Göttingen, West Germany *(Received: August 17, 1989; In Final Form: February 14, 1990)*

CH_3 yields have been measured by multiphoton ionization in the laser-induced dissociation of toluene and ethyl-benzene under collision-free conditions. At an excitation energy near 53 000 cm^{-1}, about 17% of toluene dissociate by C–C bond split whereas 83% decompose by C–H bond split. Analysis of this result by unimolecular rate theory leads to thermal branching ratios for C–C bond split which rise from 13% at 1000 K to 47% at 2000 K. The importance of rotational effects in the specific rate constant $k(E,J)$ is discussed with respect to the branching ratio.

1. Introduction

The unambiguous identification of the products of elementary chemical reactions and, in the case of branching processes, of their relative yields often presents difficulties. Under high temperature combustion conditions this problem may become particularly serious when the branching ratios of competing dissociation channels become temperature- and pressure-dependent and the products give rise to different mechanisms of secondary reactions. In this situation a method for the direct identification of primary dissociation fragments and their yields appears desirable. The present work describes such a technique which is applicable under the condition that the dissociating molecule is characterized by suitable photophysical properties.

We consider alkylbenzenes as examples of the present method. After laser irradiation at 193 nm these molecules undergo rapid internal conversion from excited electronic states to the electronic ground state such that high vibrational excitation arises. Similar energy levels as in high-temperature pyrolysis are populated; however, in photolysis the dissociation process can be studied under isolated molecule conditions. Dissociation rates and the identity of the *dominant* dissociation products have been determined in this way in part 1[1] of this series. The accuracy of these measurements, however, did not allow characterization of the *minor* channels. This requires, instead, a direct identification of the minor products such as done in the present work. Multiphoton ionization with mass spectrometric identification is used for the detection of these species. A quantitative determination is achieved by actinometric calibration of the ion signals. In addition to this, the method allows one to specify the yields of various product vibrational states and to study the energy partitioning during the dissociation.

The described technique is applied to the dissociation of toluene with the competing channels

$$C_6H_5CH_3 \rightarrow C_6H_5CH_2 + H \quad (1)$$

$$\rightarrow C_6H_5 + CH_3 \quad (2)$$

The relative yields of channels 1 and 2 have been the subject of discussions in thermal dissociation studies suggesting either channel 1[2-5] or channel 2[6] to be dominant. The temperature dependence of the ratio $k_1/(k_1 + k_2)$ was discussed recently,[7] suggesting values of 0.9 at 1000 K, 0.5 at 1500 K, and 0.32 at 2000 K. In the laser experiments from part 1[1] and refs 8–12, benzyl radicals and hydrogen atoms were identified as being the major products. The difference in the conclusions about a dominance of channel 1 or channel 2 in the pyrolysis could have been induced by mechanistic problems under the complicated thermal pyrolysis conditions. In the present work we detect CH_3 radicals under isolated molecule conditions by multiphoton ionization. The CH_3 channel has been detected before in molecular beam studies of the pyrolysis,[13,14] although details of these measurements have not yet been pub-

(1) Brand, U.; Hippler, H.; Lindemann, L.; Troe, J. *J. Phys. Chem.*, preceding paper in this issue (part 1).

(2) Brouwer, L. D.; Müller-Markgraf, W.; Troe, J. *J. Phys. Chem.* **1988**, *92*, 4905 (and references cited therein).
(3) Rao, V. S.; Skinner, G. B. *J. Phys. Chem.* **1984**, *88*, 4362.
(4) Braun-Unkhoff, M.; Frank, P.; Just, Th. *Symp. (Int) Combust. (Proc.)* **1988**, *22*, 1053, and unpublished data 1986–1989.
(5) Colket, M. *Symp. (Int.) Combust. (Proc.)* **1984**, *20*, 1032.
(6) Pamidimukkula, K. M.; Kern, R. D.; Patel, M. R.; Wei, H. C.; Kiefer, J. H. *J. Phys. Chem.* **1987**, *91*, 2148.
(7) Rao, V. S.; Skinner, G. B. *J. Phys. Chem.* **1989**, *93*, 1864 (and references cited therein).
(8) Hippler, H.; Schubert, K.; Troe, J.; Wendelken, H. J. *Chem. Phys. Lett.* **1981**, *84*, 253.
(9) Ikeda, N.; Nakashima, N.; Yoshihara, K. *J. Chem. Phys.* **1985**, *82*, 5285.
(10) Kaji, Y.; Obi, K.; Tanaka, I.; Ikeda, N.; Nakashima, N.; Yoshihara, K. *J. Chem. Phys.* **1987**, *86*, 6115.
(11) Hippler, H.; Lindemann, L.; Troe, J. *Ber. Bunsen-Ges. Phys. Chem.* **1988**, *92*, 440.
(12) Bersohn, R.; Tsukiyama, K. *J. Chem. Phys.* **1987**, *86*, 745.
(13) Krajnovich, D. J.; Buss, R. J.; Lee, Y. T. *Conf. (Int.) Photochem. (Stanford)* **1982**.
(14) Brudzinsky, R. J.; Felder, P.; Buss, R. J.; Lee, Y. T. *Conf. (Int.) Radiationless Trans. (Newport Beach)* **1984**. Brudzinsky, R. J. Ph.D. Thesis, Berkeley CA, 1987.

0022-3654/90/2094-6316$02.50/0